Cell Reports
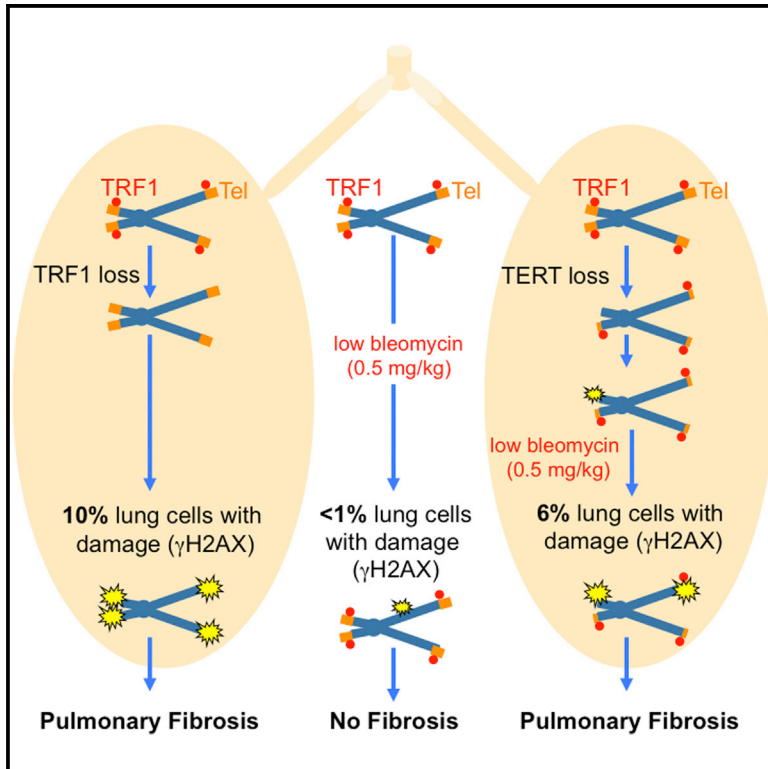
Mice with Pulmonary Fibrosis Driven by Telomere Dysfunction

Graphical Abstract

Authors

Juan M. Povedano, Paula Martinez, Juana M. Flores, Francisca Mulero, Maria A. Blasco

Correspondence

mblasco@cnio.es

In Brief

Povedano et al. show that persistent telomeric damage induced by telomere dysfunction (either by shelterin disruption or by telomerase deficiency) triggers pulmonary fibrosis in mice. These mouse models are instrumental for the development of new therapeutic strategies to treat pulmonary fibrosis associated with telomere dysfunction.

Highlights

- *Trf1* deletion alone in alveolar type II cells induces pulmonary fibrosis in mice

- Short telomeres and low-dose bleomycin induce pulmonary fibrosis in mice

- These mouse models are instrumental for the development of new therapeutic strategies

CrossMark

CellPress

Article

Mice with Pulmonary Fibrosis Driven by Telomere Dysfunction

Juan M. Povedano,[1] Paula Martinez,[1] Juana M. Flores,[2] Francisca Mulero,[3] and Maria A. Blasco[1,*]
[1]Telomeres and Telomerase Group, Molecular Oncology Program, Spanish National Cancer Centre (CNIO), Melchor Fernández Almagro 3, Madrid 28029, Spain
[2]Animal Surgery and Medicine Department, Faculty of Veterinary Science, Complutense University of Madrid, Madrid 28029, Spain
[3]Molecular Imaging Unit, Spanish National Cancer Research Centre (CNIO), Melchor Fernández Almagro 3, Madrid 28029, Spain
*Correspondence: mblasco@cnio.es
 http://dx.doi.org/10.1016/j.celrep.2015.06.028

SUMMARY

Idiopathic pulmonary fibrosis (IPF) is a degenerative disease of the lungs with an average survival post-diagnosis of 2–3 years. New therapeutic targets and treatments are necessary. Mutations in components of the telomere-maintenance enzyme telomerase or in proteins important for telomere protection are found in both familial and sporadic IPF cases. However, the lack of mouse models that faithfully recapitulate the human disease has hampered new advances. Here, we generate two independent mouse models that develop IPF owing to either critically short telomeres (telomerase-deficient mice) or severe telomere dysfunction in the absence of telomere shortening (mice with *Trf1* deletion in type II alveolar cells). We show that both mouse models develop pulmonary fibrosis through induction of telomere damage, thus providing proof of principle of the causal role of DNA damage stemming from dysfunctional telomeres in IPF development and identifying telomeres as promising targets for new treatments.

INTRODUCTION

Idiopathic pulmonary fibrosis (IPF) is a life-threatening lung degenerative disease that lacks current effective treatments (King et al., 2011). The mean survival time upon diagnosis is only 2 to 3 years (King et al., 2011). The clinical course of the disease is characterized by a progressive decline in exercise capacity, difficulty breathing, recurrent infections, and severe impairment in lung function, which makes the patients dependent on long-term oxygen treatment. IPF is characterized by the presence of lung scarring, immune infiltrates, and inflammation, which in the past two decades has led to the exploration of inflammation as a therapeutic target for treatment of the disease (Selman et al., 2001). Unfortunately, recent clinical trials for IPF patients based on immune suppression had to be interrupted owing to the toxicity of the treatment (Martinez et al., 2014). More recently, IPF has been proposed to be the result of repet-

itive epithelial cell injury and defective regeneration, but the precise molecular cause of damage or defective regeneration remains unclear (Hinz et al., 2007; Ryu et al., 2014). To date, lung transplantation is the only therapeutic option for less than 5% of IPF patients with very severe disease (Lama, 2009).

IPF is an age-associated disease, with a mean age at onset between 50 and 70 years (Armanios, 2013; King et al., 2011), and affects men more frequently than women (2:1 ratio) (King et al., 2011). Environmental factors known to inflict damage to lung epithelial cells, such as smoking, are known to increase the risk of developing IPF (Armanios, 2013; King et al., 2011).

One of the hallmarks of aging in mice and humans is the progressive shortening of telomeres with increasing age (López-Otín et al., 2013). Mammalian telomeres are protective structures at the ends of chromosomes (Blackburn, 2001; de Lange, 2005) that consist of TTAGGG repeats bound by a six-protein complex known as shelterin (de Lange, 2005). A minimum length of telomeric repeats is necessary for shelterin binding and telomere protection (Blackburn, 2001; de Lange, 2005). Telomerase (*Tert*, telomerase reverse transcriptase) is an enzyme capable of compensating the telomere attrition produced by telomere degradation and/or by the incomplete replication of telomeric repeats associated with each DNA replication cycle through de novo addition of TTAGGG repeats to the chromosome ends. To this end, telomerase uses an associated RNA component as replication template (*Terc*, telomerase RNA component) (Greider and Blackburn, 1985). In mice and humans, telomerase is silenced after birth, leading to progressive telomere shortening associated with cell division throughout the lifespan (Canela et al., 2007; Flores et al., 2008; Harley et al., 1990; Vera et al., 2012). When telomeres reach a critically short length, this triggers activation of a persistent DNA damage response at telomeres and the subsequent induction of cellular senescence or apoptosis. In the case of adult stem cells, critical telomere shortening impairs their ability to regenerate tissues both in mice and humans, leading to many different age-related pathologies (Flores et al., 2005). Interestingly, telomere shortening has been shown to be influenced both by genetic factors (ie., mutations in genes necessary for telomere maintenance) and environmental factors (ie., cigarette smoke has a negative effect) (Armanios, 2013; King et al., 2011).

Compelling evidence that telomere shortening contributes to aging and age-related disease comes from the study of humans

and mice with defective telomerase activity (Armanios and Blackburn, 2012; Blasco, 2005, 2007). In particular, the first demonstration that short telomeres were sufficient to cause age-related pathologies and decreased longevity came from a study of telomerase-deficient mice, which show premature aging phenotypes both in low-proliferating (heart and brain) and high-proliferating compartments (bone marrow, gut, skin, and testis) (Blasco et al., 1997; Ferrón et al., 2004; Herrera et al., 1999; Lee et al., 1998; Leri et al., 2003). Importantly, telomerase-deficient mice show worsening of phenotypes with increasing mouse generations owing to inherited progressively shorter telomeres, with the later generations showing severe phenotypes and premature death at pre-reproductive ages (García-Cao et al., 2002; Herrera et al., 1999; Lee et al., 1998). This phenomenon first indicated genetic anticipation associated with telomerase deficiency. In humans, a number of conditions have been also associated with mutations in telomerase and other telomere-related genes, with the most frequent condition being IPF (Armanios, 2013; Armanios and Blackburn, 2012). In particular, mutations in *Tert* and *Terc* account for 8%–15% of familial and 1%–3% of sporadic cases (Alder et al., 2008; Armanios, 2013; Armanios et al., 2007). More recently, telomerase mutations leading to abnormally short telomeres have also been found in up to 1% of smokers with chronic obstructive pulmonary disease (COPD) (Stanley et al., 2015). In addition to lung disease, humans with mutations in telomere maintenance genes show a variety of pathologies and disease states that have been collectively named "telomere syndromes" (Armanios and Blackburn, 2012) and that affect both highly proliferative (bone marrow, gut, and skin) and slow-proliferative (liver, lung, and pancreas) tissues. As in mice, disease anticipation is also found in human families with telomere syndromes, with the mutation generally first manifesting in adults with pulmonary fibrosis and the more severe phenotypes appearing in pediatric populations (immunodeficiency) and young adults (aplastic anemia) from the next generations (Armanios, 2013).

Although pulmonary fibrosis and emphysema are the most frequent manifestations of telomere defects in humans, telomerase-deficient mice with critically short telomeres do not spontaneously develop pulmonary disease. Exposure to cigarette smoke, which is known to accelerate disease onset in humans, induces emphysema in telomerase-deficient mice (Alder et al., 2011). It has recently been shown that alveolar progenitor senescence induced by telomere dysfunction is sufficient to recapitulate the regenerative defects, inflammatory responses, and susceptibility to injury that are characteristic of human telomere-mediated lung disease, although no IPF was reported in these mouse models (Alder et al., 2015). These findings suggest that additional damage, or telomere damage of higher severity, may be required for IPF onset in mice.

Thus, mouse models that more closely recapitulate the molecular features of human disease, including telomere defects, are necessary. These models will aid in our understanding of the pathobiology of IPF and will allow more efficient preclinical testing of novel therapeutic strategies. To this end, we first tested whether a source of telomere damage of a higher intensity than that achieved by telomere shortening with increasing mouse generations in the absence of telomerase was sufficient to induce IPF in mice.

In this regard, proper telomere capping requires not only a minimum length of telomere repeats but also the integrity of a six-protein complex known as shelterin, which is bound to telomeric repeats (de Lange, 2005). Out of the six shelterin components, TRF1 was the first to be identified (Chong et al., 1995). Extensive work using genetically modified mouse models has shown that *Trf1* deletion leads to an immediate and persistent DNA damage response at chromosome ends, leading to severe proliferative defects in all the tissues studied, including stem cell compartments, thus recapitulating some of the pathologies associated with telomere syndromes (Beier et al., 2012; Martínez et al., 2009; Schneider et al., 2013). Interestingly, the TRF1-interacting shelterin protein TIN2 has also been found to be mutated in telomere syndromes, indicating that severe telomere uncapping, even in the absence of telomere shortening, also leads to disease. However, the role of shelterin dysfunction in pulmonary fibrosis has not been formally addressed.

RESULTS

Trf1 Deletion in the Lung Induces Pulmonary Fibrosis and Decreases Mouse Survival

We induced severe telomere dysfunction specifically in the lungs by genetically deleting the shelterin component *Trf1* from epithelial type II alveolar cells, which have been proposed to contribute to lung progenitor cells (Desai et al., 2014; Rawlins, 2015) (Experimental Procedures). In particular, to specifically delete *Trf1* in the lungs, we generated the *Trf1^{lox/lox}* SFTPC-Cre^{ERT2} KFP^{lox-STOP-lox} mouse model. In this model, Cre recombinase expression is controlled by the surfactant protein C (SFTPC) promoter, which is specific for type II alveolar cells, and Cre^{ERT2} is conditionally activated by tamoxifen (TMX) administration (Rock et al., 2011). In addition, a transgene encoding for the fluorescent katushka (KFP) protein that contains a stop cassette flanked by lox sequences was introduced as a reporter to monitor Cre activity (Figure 1A). TMX was administered intraperitoneally (i.p.) every second day for 6 weeks to induce both *Trf1* deletion and KFP expression (Figure 1B). After 2 weeks of TMX treatment, we quantified the amount of *KFP*-positive cells in the lungs of *Trf1^{lox/lox}* SFTPC-Cre^{ERT2} KFP^{lox-STOP-lox} mice and *Trf1^{+/+}* SFTPC-Cre^{ERT2} KFP^{lox-STOP-lox} control mice by immunohistochemistry. In both genotypes, we found that 1 week after TMX treatment, ~14% of the total lung cells were KFP positive (Figure 1C; see also Figure 3F), which is in agreement with the previously reported abundance of alveolar type II cells (12%–15%) in whole lung cell populations (Dobbs, 1990; Van der Velden et al., 2013). We next confirmed *Trf1* deletion in the lungs of *Trf1^{lox/lox}* SFTPC-Cre^{ERT2} KFP^{lox-STOP-lox} mice by PCR amplification of the *Trf1^Δ* allele (Figure 1D). Triple immunofluorescence staining with SFTPC, KFP, and TRF1 antibodies clearly demonstrated that all of the SFTPC-positive cells were also KFP positive and that these cells stained negative for TRF1 in the lungs of *Trf1^{lox/lox}* mice (Figures 1E and 1F). These results indicate efficient Cre expression in alveolar type II cells and *Trf1* deletion in the lungs of *Trf1^{lox/lox}* SPC-Cre^{ERT2} KFP^{lox-STOP-lox} mice.
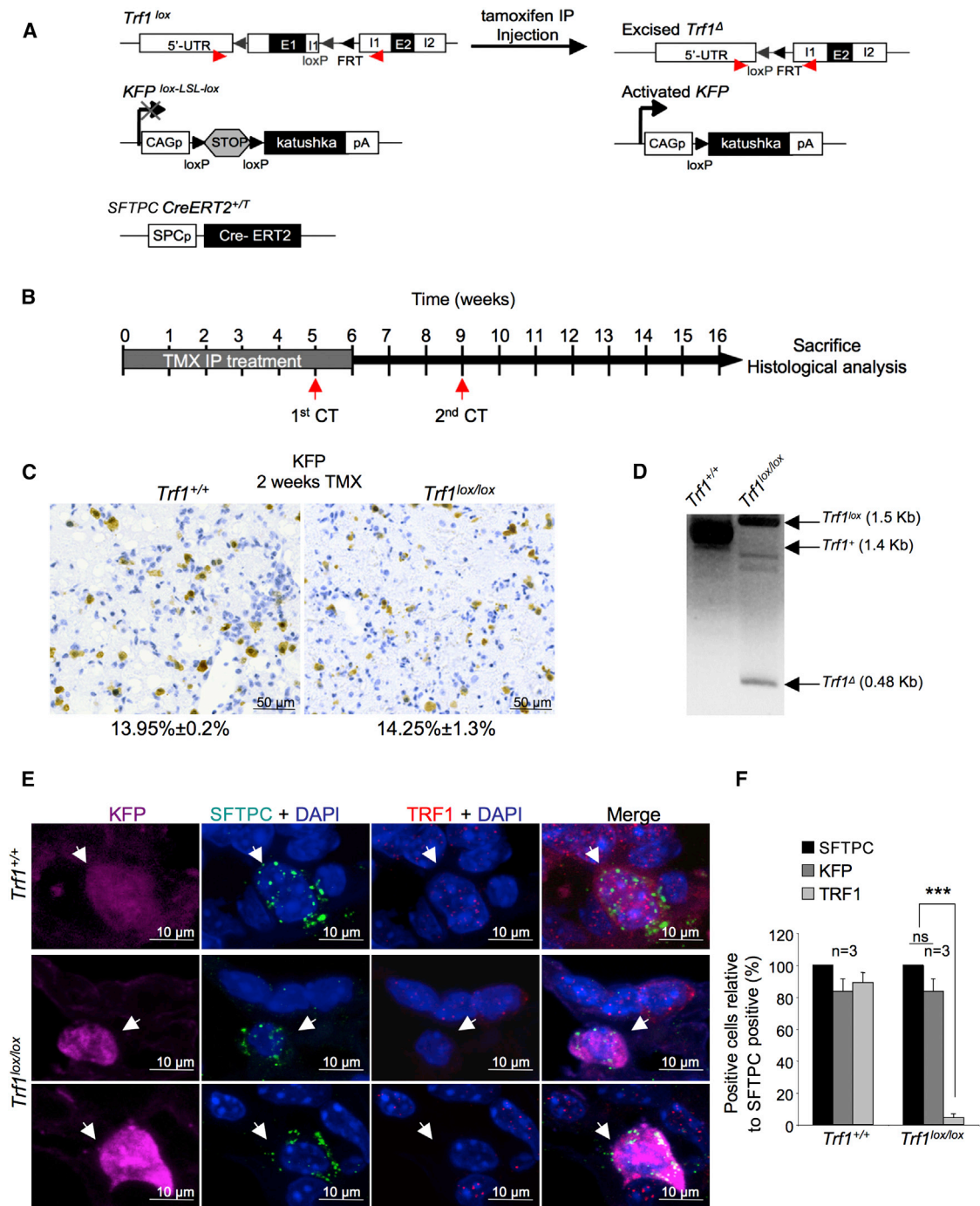
Figure 1. Efficient *Trf1* Deletion in Alveolar Type II Cells upon Tamoxifen Administration

(A) Genetic model. *Trf1^lox^*, *KFP ^Lox-STOP-Lox^*, and *SFTPC-Cre^ERT2^* alleles are depicted before and after Cre-mediated excision.

(B) Tamoxifen (TMX) intraperitoneal treatment and in vivo imaging schedule. 8- to 10-week-old mice were i.p. injected with TMX three times a week for 6 consecutive weeks. At weeks 5 and 9 from the beginning of the TMX treatment, mice were analyzed by computed tomography (CT), and at week 16, the remaining alive mice were sacrificed for histological analysis.

(C) Representative images of KFP staining of *Trf1^+/+^ SFTPC-Cre-^ERT2^ KFP^CAG-lox-STOP-lox^* and *Trf1^flox/flox^ SFTPC-Cre^ERT2^ KFP^CAG-lox-STOP-lox^* lung sections after 1 week of TMX treatment. The percentage of KFP-positive cells with regard to the total lung cell population is indicated.

(D) Analysis of *Trf1* excision by PCR in lung samples. Note that lung cell populations that are not alveolar type II give rise to *TRF1^lox^* allele amplification.

Interestingly, 4–8 weeks after TMX treatment, we observed that 42% of the TRF1-deficient mice of both genders and 65% of male mice in which we specifically deleted *Trf1* in lung epithelial alveolar type II cells showed an abnormal computed tomography (CT) pattern compatible with fibrosis, while none of the wild-type animals showed this abnormal CT pattern (Figures 2A and 2B). This abnormal radiological pattern is characterized by presence of reticular opacities with honeycombing, also typically found in human pulmonary fibrosis patients (Figure 2A) (Ryu et al., 2014). Notably, the radiologic lesions detected by CT occupied the large majority of the lungs (up to 100% of the lung volume), indicative of very severe lesions (Figure 2C). In agreement with this severity, 42% of TRF1-deficient mice had to be sacrificed during the first 8 weeks of TMX treatment owing to severe respiratory defects, characterized by the presence of labored and heavy breathing, leading to a significantly decreased survival compared to the wild-type treated controls (Figure 2D).

For definite diagnosis of pulmonary fibrosis as the cause of the abnormal radiological pattern observed in TRF1-depleted lungs, we performed full histopathology of the lungs following mouse sacrifice. As pulmonary fibrosis is characterized by formation of fibrotic scars, we determined the presence of collagen fiber deposits by using Masson trichrome staining (Experimental Procedures). We observed that more than 40% of the TRF1-deficient mice of both genders and 65% of male mice showed pathological findings characteristic of pulmonary fibrosis (Figures 2E and 2F). In particular, these mice showed extensive pneumonia (between 40% and 50% of the lung parenchyma affected), inflammatory infiltrates consisting mainly of macrophages with hemosiderin content indicative of traumatic hemorrhage, and intense inflammation that were absent in wild-type lungs (Figure 2E). Also in agreement with human findings, we detected an increased presence of macrophage infiltrates and the activation of an inflammatory response as indicated by specific staining for F4/80 and interleukin-6, respectively (Figure 2E). Deposition of collagen fibers was also visualized by sirius red staining using polarized light for detection (Experimental Procedures) (Broytman et al., 2015). We detected a 6-fold higher amount of collagen fibers in the *Trf1*-deleted fibrotic lungs compared to the wild-type controls (Figures 2G and 2H). This was also confirmed by higher collagen expression levels in TRF1-depleted lungs (Figure 2I). In addition, we also observed increased numbers of α-smooth muscle actin (α-SMA)-positive myofibroblasts, which have been associated with fibrotic lungs (Zhang et al., 1996) (Figures 2J and 2K). Together, these findings confirm extensive fibrosis as a consequence of TRF1 depletion in alveolar type II cells.

Trf1 Deletion in Alveolar Type II Cells Leads to Cell Death without Inducing Telomere-Length Changes in Lung Cells

Next, we investigated the underlying molecular consequences of *Trf1* deletion in the lung that trigger disease. First, we considered the hypothesis that TRF1 deficiency may lead to decreased telomere length by forcing extra proliferation of the remaining, non-*Trf1*-deleted lung epithelial cells. In particular, we recently described that *Trf1* deletion in the bone marrow led to depletion of the stem cell compartment and to extra proliferation of the remaining non-*Trf1*-deleted progenitor cells, leading to very rapid telomere shortening in the bone marrow (Beier et al., 2012). To this end, we performed telomere quantitative fluorescence in situ hybridization (qFISH) directly on lung sections (Experimental Procedures). However, we did not detect decreased telomere fluorescence in the TRF1-depleted lungs at the time of onset of pulmonary fibrosis (5–8 weeks after induction of deletion) compared to the wild-type controls. In particular, we did not observe differences either in the mean telomere spot fluorescence intensity or in the mean total nuclear telomere fluorescence between TMX-treated *Trf1*^lox/lox^ *SPC-Cre*^ERT2^ *KFP*^lox-STOP-lox^ mice and wild-type controls (Figures 3A, 3B, and 3E). Similarly, we did not observe an increased frequency of telomere spots with low fluorescence (<50 and <60 arbitrary units of fluorescence) corresponding to the 10th and 20th percentile of the wild-type telomere fluorescence distribution in the TRF1-deleted lungs, which is indicative of the presence of very short telomeres (Figures 3C–3E). These results are in agreement with the fact that the lung is a low-proliferative compartment with a cell turnover estimated to be less than 2% per week in alveolar epithelial cells (Alder et al., 2011).

Interestingly, we observed that the initial amount of KFP-positive cells (15% for both genotypes) dramatically decreased in *Trf1*-deleted lungs compared to wild-type lungs 6–8 weeks after TMX treatment (Figures 3F and 3I), which strongly suggests elimination of alveolar type II cells as a consequence of *Trf1* deletion. Indeed, at the death point, while 12% of alveolar type II cells in *Trf1* wild-type lungs were KFP positive (Dobbs, 1990; Van der Velden et al., 2013), less than 5% of alveolar type II cells in *Trf1*-deleted fibrotic lungs were KFP positive, indicating that two-thirds of these cells were eliminated during the course of the experiment (Figures 3F and 3I). Abrogation of TRF1 in proliferative tissues such as the stratified epithelia induces telomeric DNA damage and a rapid DNA damage response characterized by the activation of p53/p21 pathways (Martínez et al., 2009). Immunohistochemistry analysis of lung sections readily revealed that the number of p53- and p21-positive cells significantly increased in TRF1-depleted alveolar type II cells, indicative of cellular senescence (Figures 3G–3I). The number of p21-positive cells relative to KFP-positive cells progressively increased throughout the course of the experiment. Further supporting induction of cellular senescence, we also detected increased numbers of the p19 protein in TRF1-depleted lungs (Figures 3H and 3I) (Collado et al., 2007). In addition, we also detected increased numbers of active caspase 3 (C3a)-positive cells in TRF1-depleted lungs, indicative of apoptosis (Figures 3H and 3I). Thus, both senescence markers and apoptosis

---

(E) Representative images of triple-immunofluorescence staining of KFP (purple), SFTPC (green), and TRF1 (red) *Trf1*^+/+^ *SFTPC-Cre*^ERT2^ *KFP*^CAG-lox-STOP-lox^ and *Trf1*^flox/flox^ *SFTPC-Cre*^ERT2^ *KFP*^CAG-lox-STOP-lox^ lung sections after 2 weeks of TMX treatment.
(F) Quantification of the percentage of KFP- and TRF1-positive cells with regard to SFTPC-positive cells. A t test was used for statistical analysis. Error bars represent SE. The number of mice analyzed per genotype is indicated. ***p < 0.001.
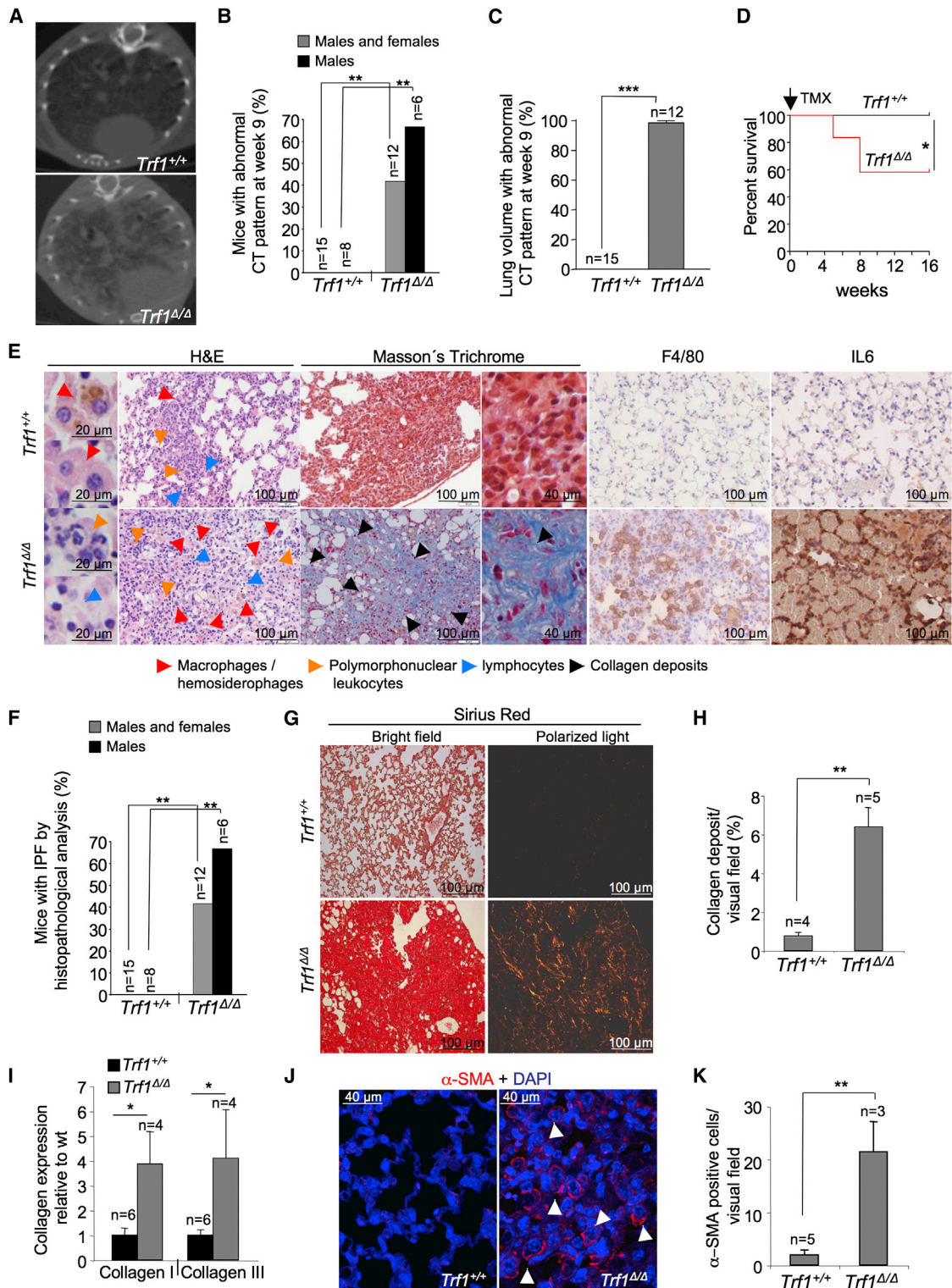
Figure 2. *Trf1* Deletion in the Lung Induces Pulmonary Fibrosis and Decreases Mouse Survival

(A) Representative CT images of $Trf1^{+/+}$ and affected $Trf1^{\Delta/\Delta}$ lungs.

(B) Percentage of mice of both genders or only males with an abnormal CT pattern at week 9 after the beginning of TMX treatment. An χ^2 test was used for statistical analysis.

(C) Quantification of the affected lung volume. A t test was used for statistical analysis.

are induced as a consequence of TRF1 ablation in alveolar type II cells.

Double-immunofluorescence staining with γH2AX and TRF1 antibodies showed a significant progressive increase in the number of γH2AX-positive damaged cells (reaching 10% of the total lung cell population 6–8 weeks after the beginning of TMX treatment) that were negative for TRF1 staining, demonstrating that TRF1 abrogation results in telomeric DNA damage (Figures 3J and 3K). Given that wild-type lungs did not appear to have damaged cells (<1% of total lung cells) and the percentage of damaged cells in *Trf1*-deleted lungs (10%) was similar to the total number of alveolar type II cells (10%–15%) (Dobbs, 1990; Van der Velden et al., 2013), our observations suggest that at least 90% of the total alveolar type II cells lacking TRF1 show DNA damage. This increase in γH2AX-positive cells could also be a consequence of the anticipated inflammatory response observed in TRF1-deficient lungs (Figure 2E).

In summary, these findings demonstrate that acute telomere dysfunction in lung epithelial cells, such as that triggered by abrogation of the TRF1 shelterin component in alveolar type II cells, is sufficient to rapidly induce massive pulmonary fibrosis in mice through induction of DNA damage, p21/p53 cell-cycle inhibitors, and elimination of alveolar type II cells. Thus, we have generated a mouse model that develops IPF induced by telomere defects in the absence of additional damaging agents. These findings also highlight the involvement of alveolar type II cells in the development of pulmonary fibrosis.

A Low Bleomycin Dose Synergizes with Short Telomeres to Trigger Pulmonary Fibrosis

As pulmonary fibrosis induced by TRF1 deletion, although a consequence of severe telomere dysfunction, did not present with one of the features of human IPF associated with telomere syndromes (namely, the presence of short telomeres), we next sought to develop a mouse model for IPF based on telomerase deficiency that recapitulates the short telomere phenotype. As mentioned above, previous reports have shown that mice deficient for the telomerase RNA essential component Terc (*Terc*^{−/−}) do not spontaneously develop IPF and that emphysema is the only pulmonary pathology that develops, even when they are subjected to additional cellular damaging agents, such as cigarette smoke (Alder et al., 2011).

Based on the results obtained with the TRF1-deficient model, which suggested that a high burden of telomeric DNA damage in alveolar type II cells (>90% of these cells with damage) was sufficient to trigger full-blown pulmonary fibrosis, we reasoned that

application of DNA-damaging agents to telomerase-deficient mice with short telomeres may be sufficient to increase the burden of DNA damage in the lungs of these mice and to trigger pulmonary fibrosis.

In this regard, bleomycin is widely used to induce acute pulmonary fibrosis in mice (Mouratis and Aidinis, 2011). In particular, treatment of wild-type mice with a single dose of 2.5 g/kg body weight (BW) bleomycin leads to development of severe fibrotic lesions in the lung as early as 2 weeks post-treatment. However, upon removal of the treatment, these lesions do not progress in time, and many of them eventually regress, most likely owing to lung regeneration by the non-affected cells (Mouratis and Aidinis, 2011). This fact has been an important shortcoming for the use of bleomycin-induced pulmonary fibrosis mouse models for the development of new treatments.

Here, we subjected *Tert*^{−/−} mice from the second and fourth generations (G2 and G4, respectively) with progressively shorter telomeres, as well as wild-type controls, to a small dose of bleomycin that is not sufficient to induce pulmonary fibrosis in wild-type mice but could perhaps synergize with short telomeres in the context of the telomerase-deficient background (Blasco et al., 1997) (Figures 4A–4C). To determine the maximum bleomycin dose that does not induce pulmonary fibrosis in wild-type mice, we subjected wild-type mice to 2.5 mg/kg BW, 1 mg/kg weight, 0.5 mg/kg BW, and 0.1 mg/kg BW bleomycin and found that the maximum dose that did not induce pulmonary fibrosis was 0.5 mg/kg BW (Figure 4C). Thus, we selected this low dose of bleomycin for further experiments. We first subjected second-generation (G2) and G4 *Tert*^{−/−} mice, as well as wild-type controls, to 0.5 mg/kg BW bleomycin and radiologically followed their lungs by CT (Figure 4B). Two to four weeks after treatment with low doses of bleomycin, we observed that 30% and 25% of G2 and G4 *Tert*^{−/−} mice, respectively, compared to 10% of wild-type control mice, presented abnormal radiological images of the lung (Figures S1A and S1B). When only males were taken into account, we observed that 50% and 45% of G2 and G4 *Tert*^{−/−} mice, respectively, compared to 20% of wild-type control mice, presented abnormal radiological images of the lung, indicating a tendency toward more *Tert*^{−/−} males than females presenting abnormal CT patterns (Figures S1A and S1B). Interestingly, we noted that these abnormal CT pattern disappeared with time in the case of wild-type mice, indicating that they could correspond to an inflammatory reaction to bleomycin treatment. In contrast, after 10 weeks, both G2 and G4 *Tert*^{−/−} mice showed an abnormal CT pattern in ~50% of the affected initial lung volume suggestive of pulmonary fibrosis (Figure S1C).

(D) Survival curve of *Trf1*^{+/+} (n = 15) and *Trf1*^{Δ/Δ} (n = 12) mice. A log-rank test was used for statistical analysis of the survival curve.

(E) Representative H&E, Masson's trichrome, F4/80, and interleukin-6 staining images of *Trf1*^{+/+} and affected *Trf1*^{Δ/Δ} lungs. Different types of infiltrates including macrophages and hemosiderophages (red arrowheads), polymorphonuclear leukocytes (orange arrowheads), lymphocytes (blue arrowheads), and collagen deposits (black arrowheads) are indicated. Amplified Masson trichrome images are shown.

(F) Percent of mice of both genders or only males diagnosed with pulmonary fibrosis by histopathological analysis. A t test was used for statistical analysis.

(G) Representative images of *Trf1*^{+/+} and affected *Trf1*^{Δ/Δ} lung sections stained with sirius red and visualized by bright-field and polarized light, where collagen fibers are bright orange.

(H) Percentage of lung area filled with collagen fibers.

(I and J) Representative image and quantification of α-SMA-positive myocyte staining.

(K) Transcriptional levels of collagen expression of collagen in *Trf1*^{+/+} and affected *Trf1*^{Δ/Δ} lungs. A t test was used for statistical analysis.

Error bars represent SE. The number of mice analyzed per genotype is indicated. *p = 0.05; **p < 0.01; ***p < 0.001.
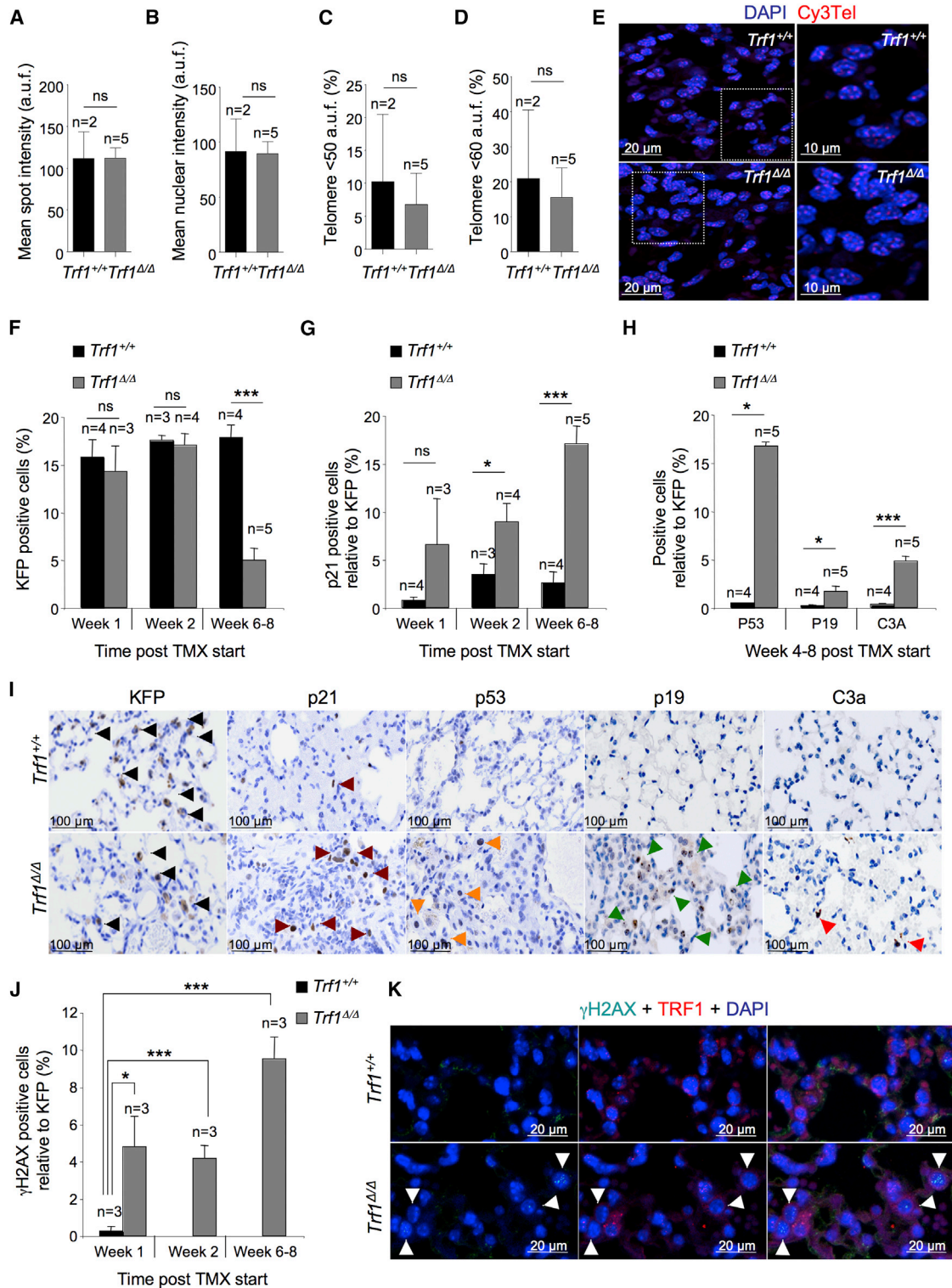
Figure 3. *Trf1* Deletion in Alveolar Type II Cells Leads to Cell Death without Inducing Telomere-Length Changes in Lung Cells

(A–D) Individual mean telomere length (A), total mean nuclear telomere length (B), percentage of short telomeres <50 arbitrary units of fluorescence (a.u.f.) corresponding to the 10th percentile of wild-type telomere distribution (C), and percentage of short telomeres <60 a.u.f. corresponding to the 20th percentile of wild-type telomere distribution (D) in *Trf1*^{+/+} and *Trf1*[Δ/Δ] lungs.

(E) Representative images of telomere qFISH analysis.

(legend continued on next page)

To confirm presence of lung disease, we performed full histo-pathological analysis of the lungs from fourth to tenth week post treatment and used Masson trichrome staining to highlight fibrotic areas. Strikingly, 50%–25% of G2 and G4 $Tert^{-/-}$ mice subjected to low-dose bleomycin presented with chronic multi-focal pneumonia and extensive moderate fibrosis, while none of the untreated G2 and G4 $Tert^{-/-}$ male mice and none of the wild-type mice (both treated and untreated) examined showed lung fibrosis (Figures 4D and 4E). As observed in the TRF1-deficient model, we observed a gender bias toward more males showing pulmonary fibrosis. In addition, macrophage infiltrates and the induction of an inflammatory response, as determined by F4/80 and interleukin-6 staining, respectively, were readily revealed in G2$Tert^{-/-}$ and G4$Tert^{-/-}$ lungs treated with bleomycin but absent in wild-type controls (Figure 4F). These findings were further validated by determination of collagen fibers using sirius red staining visualized by polarized light, which revealed ∼3-fold higher collagen deposits in the treated G2 and G4 $Tert^{-/-}$ mice as compared to untreated controls or wild-type mice (both treated and untreated) (Figures 4G and 4H). Higher collagen expression levels were also confirmed by RT-PCR in the telomerase-deficient lungs (Figure 4I). Furthermore, we detected increased numbers of α-SMA-positive myofibroblasts in telomerase-deficient mice treated with bleomycin, which are indicative of lung fibrosis (Zhang et al., 1996) (Figures 4J and 4K).

In agreement with the presence of pulmonary fibrosis in the treated $Tert^{-/-}$ mice, G2 and G4 $Tert^{-/-}$ mice presented significantly altered respiratory parameters when subjected to spirometry compared with their corresponding untreated controls or wild-type mice (Experimental Procedures). In particular, prior to sacrifice, late-generation G2 $Tert^{-/-}$ mice showed significantly decreased tidal volume, inhaled minute volume, and expiration influx compared to their corresponding untreated controls and both treated and untreated wild-type mice (Figures 5A–5C).

To further investigate whether pulmonary fibrosis and lung function impairment in G2 and G4 $Tert^{-/-}$ mice were accompanied by the presence of short telomeres, we performed telomere qFISH directly on lung sections (Experimental Procedures). As expected, G2 and G4 $Tert^{-/-}$ mice showed significantly lower individual telomere spot fluorescence and lower mean telomere nuclear intensity as compared to wild-type controls. In addition, a higher percentage of telomeres showing low fluorescence (<20 and <25 arbitrary units of fluorescence, corresponding to the 10th and 20th percentile of the G2 $Tert^{-/-}$ telomere distribution) was observed in G2 and G4 $Tert^{-/-}$ cohorts as compared to wild-type controls (Figures 5D–5H). Interestingly, treatment with a low dose of bleomycin did not affect either mean telomere

fluorescence or the percent of telomeres with low fluorescence in wild-type mice, indicating that this cellular damaging agent does not include telomere shortening (Figures 5D–5H). Bleomycin-treated G2 and G4 $Tert^{-/-}$ mice showed a tendency toward lower telomere fluorescence compared with untreated controls, most likely as a consequence of additional cell divisions in the absence of telomerase, but this trend did not reach statistical significance (Figures 5D–5H). These results indicate that development of pulmonary fibrosis in G2 and G4 $Tert^{-/-}$ mice treated with a low dose of bleomycin requires of the presence of short telomeres, as similarly treated wild-type mice do not develop the disease. Nevertheless, the feature of having short telomeres is not sufficient for disease onset and requires additional damage. These results are in line with human findings showing that damaging agents such as smoking increase the risk of developing pulmonary fibrosis associated with aging or telomerase mutations (Armanios, 2013).

Bleomycin Enhances the DNA Damage Response in the Lungs of Telomerase-Deficient Mice

To determine the amount of DNA damage induced by Tert deficiency versus the combination of Tert deficiency and bleomycin, we first studied presence of DNA damage foci (γH2AX) directly on lung sections, as well as the presence of the senescence-associated markers p21, p53, and p19 and the apoptotic marker active caspase-3 (C3a). Of note, bleomycin treatment induced DNA damage in all three genotypes (Figures 6A and 6F). Interestingly, the burden of DNA damage was much higher in the G2 and G4 $Tert^{-/-}$ mice treated with bleomycin (∼5% of total lung cells in both cases) than in the untreated controls (less than 2% in both cases) and was also higher than in the treated wild-type mice (less than 1%) (Figures 6A and 6F). The increase in DNA damage burden in bleomycin-treated G2-G4 Tert-deficient mice was accompanied by increased percentage of cells with staining positive for p53, p21, and p19, three well-established markers of cell-cycle arrest and cellular senescence (Figures 6B–6D and 6F). Similar to TRF1-depleted lungs, cell death by an apoptotic mechanism was also revealed, as judged by the increase in the number of C3a-positive cells in bleomycin-treated Tert-deficient lungs (Figures 6E and 6F).

DISCUSSION

Our results show that severe telomere dysfunction, such as that associated with TRF1 deficiency, which induces a high burden of telomere-induced DNA damage (up to 10% of all lung cells and >90% of alveolar type II cells), is sufficient for the

(F) Quantification of KFP-positive cells in $Trf1^{+/+}$ and $Trf1^{\Delta/\Delta}$ lungs after 1, 2, and 6–8 weeks of tamoxifen (TMX) treatment.
(G) Quantification of p21-positive cells in $Trf1^{+/+}$ and $Trf1^{\Delta/\Delta}$ lungs after 1, 2, and 6–8 of TMX treatment.
(H) Quantification of p53, p19 and C3a positive cells in $Trf1^{+/+}$ and $Trf1^{\Delta/\Delta}$ lungs after 6–8 weeks of TMX treatment.
(I) Representative images of KFP (black arrowheads), p21 (purple arrowheads), p53 (orange arrowheads), p19 (green arrowheads), and C3a (red arrowheads) immunohistochemistry analysis of $Trf1^{+/+}$ and $Trf1^{\Delta/\Delta}$ lungs 6–8 weeks after the beginning of TMX treatment.
(J) Quantification of γH2AX-positive cells in $Trf1^{+/+}$ after 1 week TMX treatment and in $Trf1^{\Delta/\Delta}$ lungs after 1, 2, and 6–8 weeks of TMX treatment.
(K) Representative images of double immunofluorescence of γH2AX and TRF1 in $Trf1^{+/+}$ and $Trf1^{\Delta/\Delta}$ lungs after 6–8 weeks of TMX treatment. Notice that γH2AX-positive cells stain negative for TRF1 in $Trf1^{\Delta/\Delta}$ lung sections (white arrowheads).
p21-, p53-, and γH2AX-positive cells in (G), (H), and (J) are normalized to the number of KFP-positive cells. A t test was used for statistical analysis. Error bars represent SE. The number of mice analyzed per genotype is indicated. *p = 0.05; **p < 0.01; ***p < 0.001.
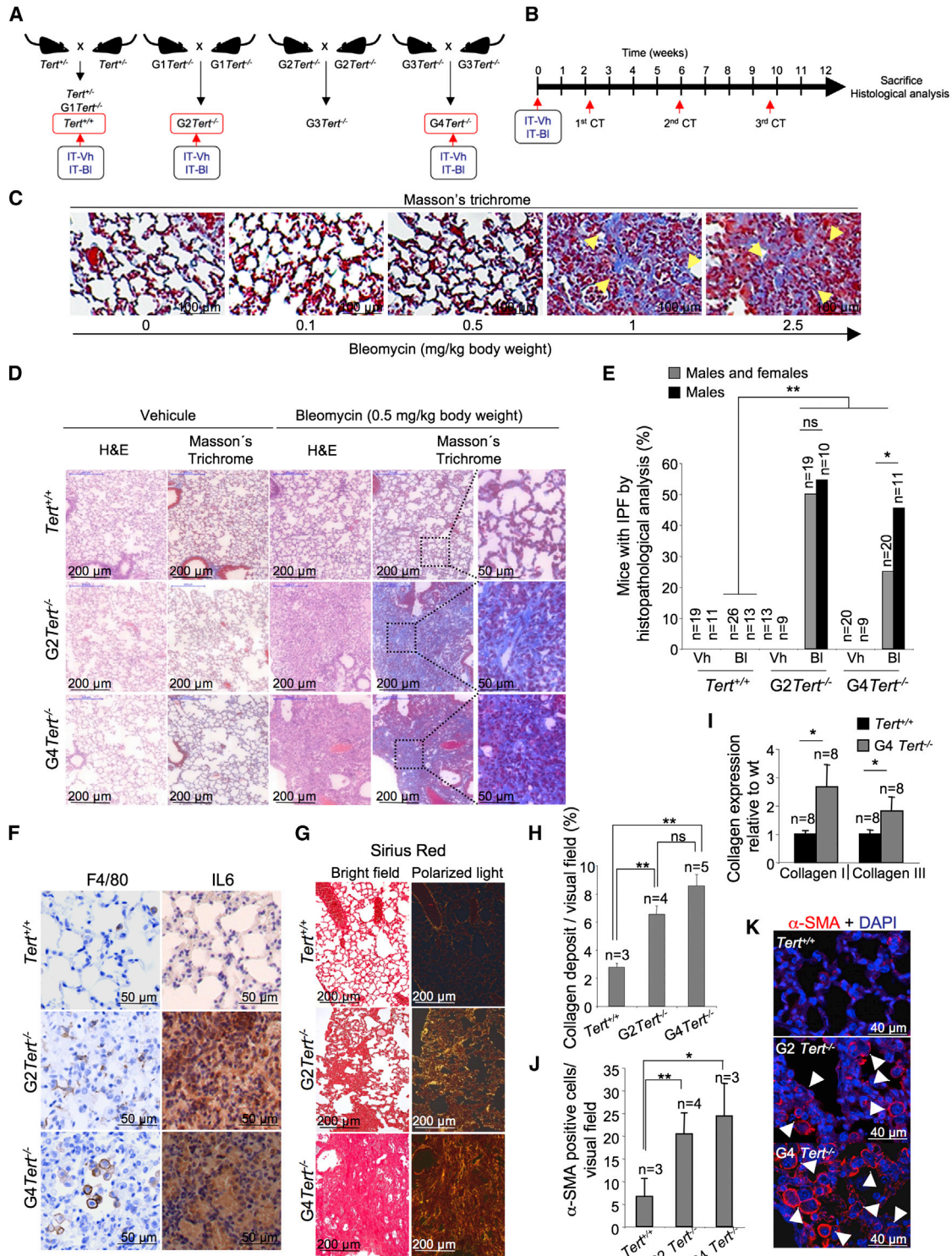
Figure 4. A Low Bleomycin Dose Synergizes with Short Telomeres to Trigger Pulmonary Fibrosis

(A) Heterozygous *Tert*⁺/⁻ mice were intercrossed to generate *Tert*⁺/⁺ and G1*Tert*⁻/⁻ mice. Successive crosses between G1*Tert*⁻/⁻ and G3*Tert*⁻/⁻ were set to generate *G2 Tert*⁻/⁻ and G4*Tert*⁻/⁻ cohorts, respectively. 8- to 10-week-old *Tert*⁺/⁺, G2*Tert*⁻/⁻, and G4*Tert*⁻/⁻ mice were intratracheally inoculated either with vehicle (PBS) (IT-Vh) or 0.5 mg/kg BW bleomycin (IT-Bl).

(B) In vivo follow-up of different mouse cohorts. At weeks 2, 6, and 10, mice were analyzed by computed tomography (CT), and at week 12, mice were sacrificed for histological analysis.

(legend continued on next page)
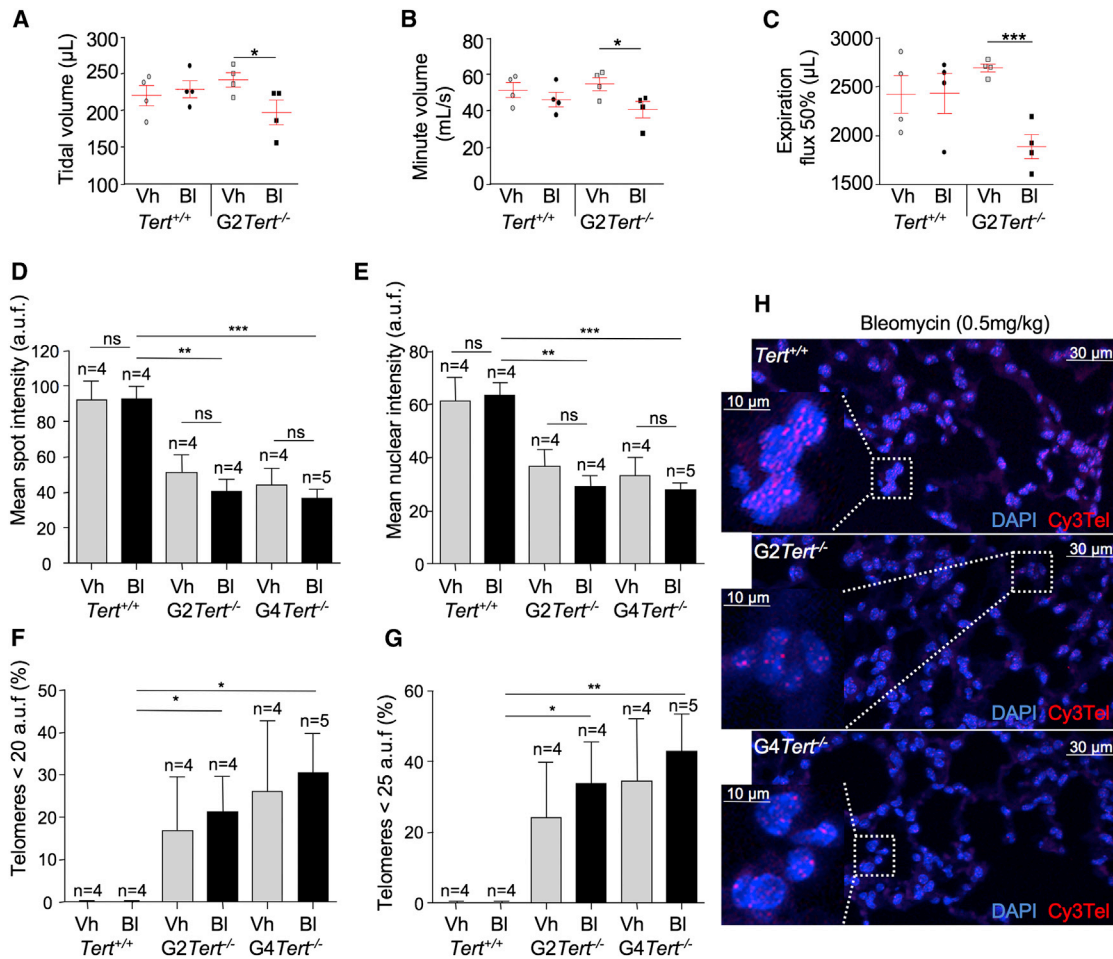
Figure 5. Decreased Pulmonary Capacity and Telomere Shortening in Lung Tissues of Telomerase-Deficient Mice

(A–C) Analysis of tidal volume (A), minute volume (B), and expiration flux at 50% (C) in $Tert^{+/+}$ and $G2Tert^{-/-}$ mice treated with either vehicle or 0.5 mg/kg BW bleomycin.

(D–G) Individual mean telomere length (D), total mean nuclear telomere length (E), percentage of short telomeres <20 a.u.f. corresponding to the 10th percentile of G2 $Tert^{-/-}$ telomere distribution (E), and percentage of short telomeres <25 a.u.f. corresponding to the 20th percentile of G2 $Tert^{-/-}$ telomere distribution (G) in $Tert^{+/+}$, $G2Tert^{-/-}$, and $G4Tert^{-/-}$ mice intratracheally inoculated either with vehicle (PBS) or 0.5 mg/kg BW bleomycin.

(H) Representative images of telomere qFISH analysis in $Tert^{+/+}$, $G2Tert^{-/-}$, and $G4Tert^{-/-}$ bleomycin-treated lungs. Amplified images are shown in the insets. A t test was used for statistical analysis. Error bars represent SE. The number of mice analyzed per genotype is indicated. *p = 0.05; **p < 0.01; ***p < 0.001.

development of pulmonary fibrosis (Figure 7). In the case of short telomeres owing to telomerase deficiency, however, additional damage was required to develop full-blown pulmonary fibrosis (Figure 7). In both models, we observed activation of the p53/ p21 and p19ARF pathways, resulting in cell senescence and apoptosis that lead to almost complete loss of alveolar type II cells in the $Trf1$-deficient model. As both TERT and TRF1 deficiencies were previously shown to lead to decreased

(C) Determination of the maximum bleomycin dose that does not induce pulmonary fibrosis in wild-type mice. Representative image of wild-type lung sections 2 weeks after intratracheal inoculation of bleomycin at a dose of 2.5 mg/kg BW, 1 mg/kg BW, 0.5 mg/kg BW, 0.1 mg/kg BW, or 0.0 mg/kg BW.

(D) Representative H&E and Masson trichrome staining images of $Tert^{+/+}$, $G2Tert^{-/-}$, and $G4Tert^{-/-}$ mice inoculated with either vehicle or 0.5 mg/kg BW bleomycin. To the right, amplified Masson trichrome images are shown.

(E) Percentage of mice of both genders or only males diagnosed with pulmonary fibrosis by histopathological analysis.

(F and G) Representative images of $Tert^{+/+}$, $G2Tert^{-/-}$, and $G4Tert^{-/-}$ lung sections inoculated with 0.5 mg/kg BW bleomycin stained with F4/80 and interleukin-6 (F) and sirius red and visualized by bright-field and polarized light, where collagen fibers are bright orange (G).

(H) Percentage of lung area filled with collagen fibers.

(I and J) Quantification of α-SMA-positive myofibroblasts (I) and representative images of wild-type, G2 $Tert^{-/-}$, and G4 $Tert^{-/-}$ lungs treated with bleomycin (J).

(K) Transcriptional levels of collagen expression in $Tert^{+/+}$, $G2Tert^{-/-}$, and $G4Tert^{-/-}$ bleomycin-treated lungs.

A t test was used for statistical analysis. Error bars represent SE. The number of mice analyzed per genotype is indicated. *p = 0.05; **p < 0.01; ***p < 0.001.
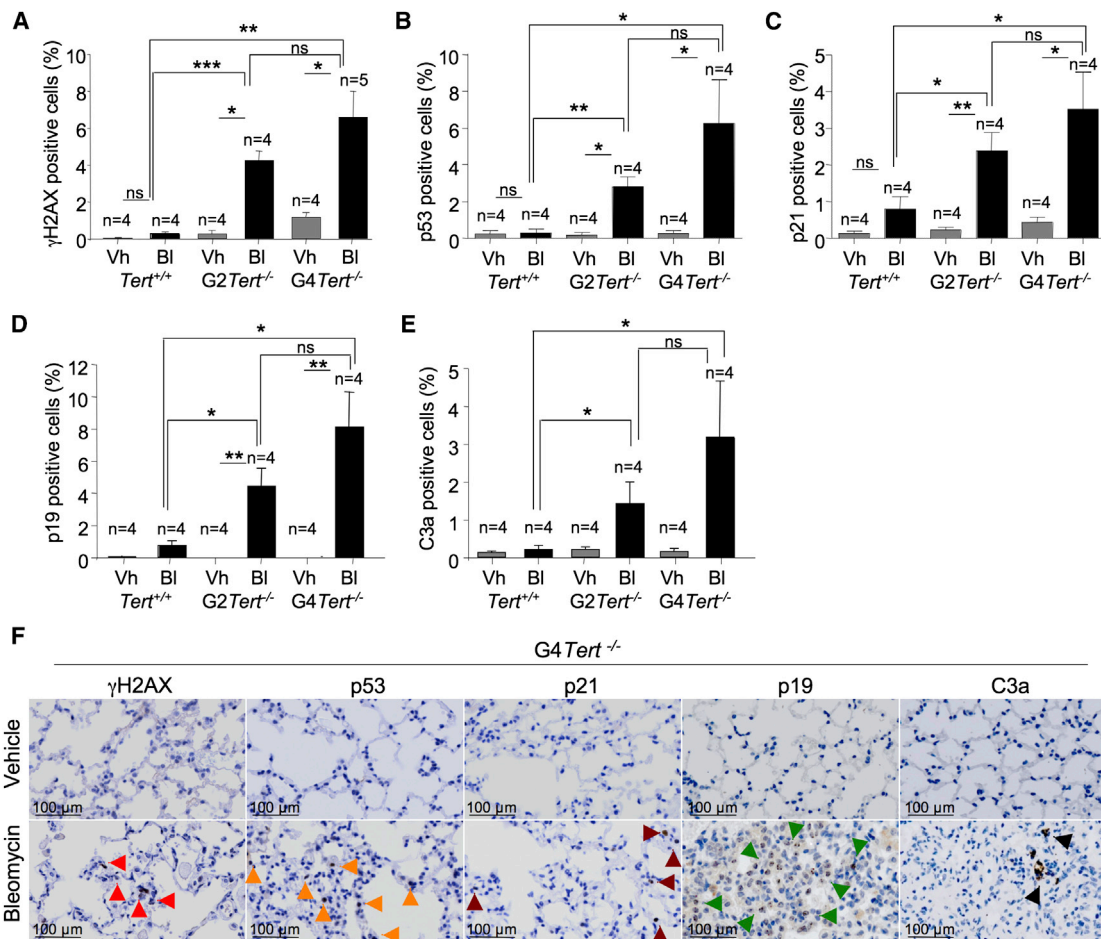
Figure 6. Bleomycin Enhances the DNA Damage Response in the Lungs of Telomerase-Deficient Mice

(A–E) Quantification of γH2AX- (A), p53- (B), p21- (C), p19- (D), and C3a-positive (E) cells in $Tert^{+/+}$, $G2Tert^{-/-}$, and $G4Tert^{-/-}$ lungs inoculated either with vehicle (PBS) or with 0.5 mg/kg BW bleomycin at time of death.

(F) Representative images of γH2AX, p53, p21, p19, and C3a immunohistochemistry staining in $G4Tert^{-/-}$ lungs inoculated either with vehicle (PBS) or with 0.5 mg/kg BW bleomycin at time of death. A t test was used for statistical analysis.

Error bars represent SE. The number of mice analyzed per genotype is indicated. *p = 0.05; **p < 0.01; ***p < 0.001.

ability of stem cells to regenerate tissues (Flores et al., 2005; Schneider et al., 2013), increased cell loss associated to severe telomere dysfunction is likely to trigger aberrant lung healing by fibroblasts, eventually leading to scar formation and pulmonary fibrosis. Based on our results, a DNA damaged burden above a certain threshold (in both models was between 5% and 10% of total lung cells showing DNA damage), combined with defective stem cell regeneration ability, may lead to development of pulmonary fibrosis. Interestingly, we also found that female mice were more resistant than male mice to induction of pulmonary fibrosis associated with telomere dysfunction in the TERT-deficient model, thus recapitulating the human observations. Our results clearly demonstrate that induction of telomere dysfunction upon *Trf1* deletion in type II alveolar cells is sufficient to induce pulmonary fibrosis. In the case of the telomerase-deficient mouse model, it is likely that application of low-dose bleomycin induces DNA damage

genome-wide, and telomere dysfunction might not constitute the only driving pathogenic mechanism underlying pulmonary fibrosis.

Our results and those of others show that treatment with a high bleomycin dose (>1 mg/kg) induces DNA damage above the tolerated threshold in wild-type mice, leading to pulmonary fibrosis in both wild-type and TERT-knockout mice (Degryse et al., 2012). However, a low bleomycin dose, such as the one used here, is well tolerated by wild-type mice but causes pulmonary fibrosis in telomerase-knockout mice that present a basal DNA damage due to short telomeres. In a previous study, it was reported that telomerase activity was required for bleomycin-induced pulmonary fibrosis in mice (Liu et al., 2007). These results stand in contrast with both our work and that of Degryse et al. (Degryse et al., 2012), since telomerase deficiency never led to protection from fibrosis development. In a recent study, it was shown
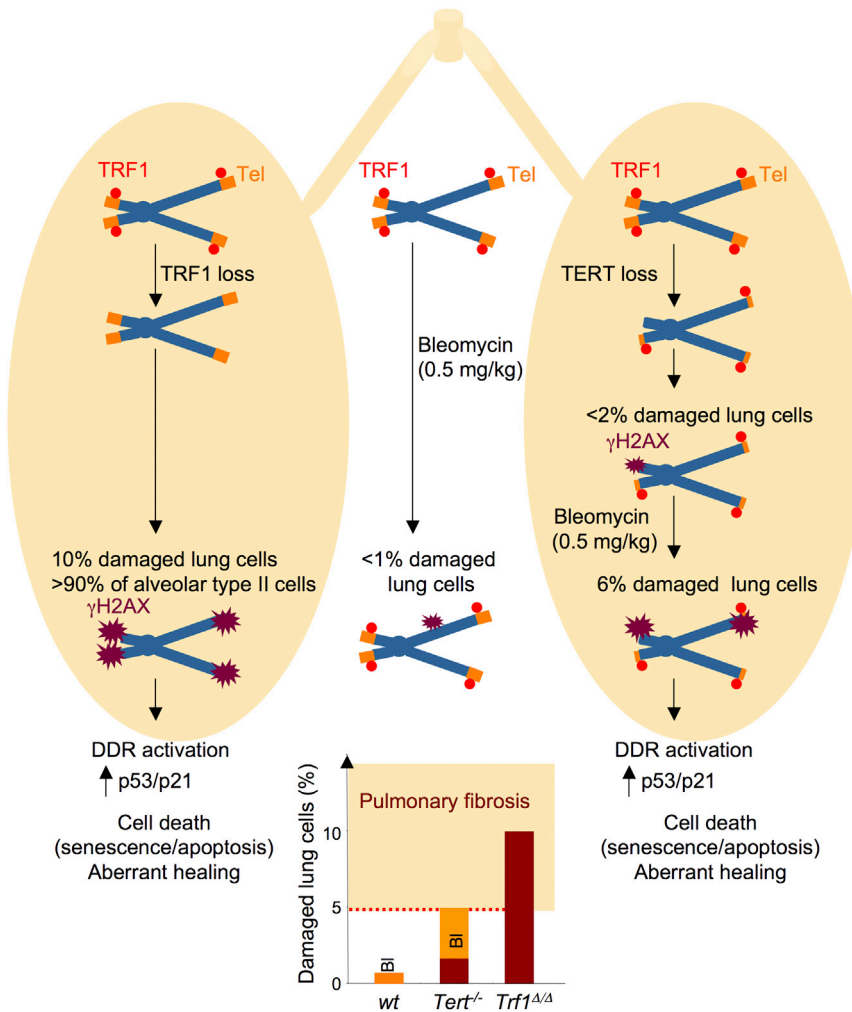
Figure 7. Model for Pulmonary Fibrosis Associated with Telomeric DNA Damage

Depletion of TRF1 protein (red circle) from telomeres (orange rectangle) in lung alveolar type II cells leads to a persistent and severe DNA damage response at telomeres characterized by increased γH2AX (purple star) in 10% of total lung cells and up to 90% of alveolar type II cells and activation of the p53/p21 pathway. Application of a low dose of bleomycin (0.5 mg/kg BW) to wild-type lungs does not lead to a significant increase in the number of damaged cells (less than 1% of total lung cells). The same bleomycin dose in telomerase-deficient mice with short telomeres significantly enhances the DNA damage burden in lung cells, with 6% of total lung cells showing DNA damage, and leads to activation of the p53/p21 pathway. In both models, cell loss mediated by senescence and apoptosis and impaired regeneration may lead to aberrant lung healing and formation of fibrotic stars.

DNA damage in the genome. Finally, the mouse models generated here are instrumental for the preclinical testing of therapeutic strategies based in telomerase activation or correction of telomere uncapping.

EXPERIMENTAL PROCEDURES

Mice and Animal Procedures

$Trf1^{flox/flox}$ mice were generated as described previously (Martínez et al., 2009). To conditionally delete $Trf1$ from alveolar epithelial type II (AEC II) cells, homozygous $Trf1^{flox/flox}$ mice were crossed with transgenic mice expressing Cre-ERT2 under the control of the SFTPC promoter (Rock et al., 2011) as well as with transgenic mice harboring the fluorescent KFP protein-encoding gene that contains a stop cassette flanked by lox sequences, the $KFP^{CAG-lox-STOP-lox}$ allele (Diéguez-Hurtado et al., 2011). Heterozygous $Trf1^{flox/+}$ SFTPC-Cre^{ERT2} $KFP^{CAG-lox-STOP-lox}$ mice were crossed with $Trf1^{+/flox}$ mice to obtain $Trf1^{+/+}$ SFTPC-Cre^{ERT2} $KFP^{CAG-lox-STOP-lox}$ and $Trf1^{flox/flox}$ SFTPC-Cre^{ERT2} $KFP^{CAG-lox-STOP-lox}$ mice.

Tert-Knockout and Wild-Type Mice

Wild-type mice and $Tert^{-/-}$ mice of pure C57/BL6 background were used for the bleomycin intratracheal inoculation procedure. $Tert$-heterozygous mice generated as previously described (Liu et al., 2000) were backcrossed to >98% C57/BL6 background. $Tert^{+/-}$ mice were intercrossed to generate G1 homozygous $Tert^{-/-}$-knockout mice. G2 and G4 $Tert^{-/-}$ mice were generated by successive breeding of G1$Tert^{-/-}$ and G3$Tert^{-/-}$ mice, respectively.

All mice were produced and housed at the specific-pathogen-free barrier area of the CNIO, Madrid. All animal procedures were approved by the CNIO-ISCIII Ethics Committee for Research and Animal Welfare (CEIyBA) and conducted in accordance to the recommendations of the Federation of European Laboratory Animal Science Associations (FELASA).

TMX Treatment

TMX was dissolved in corn oil to a concentration of 20 μg/μl. 8- to 10-week-old $Trf1^{flox/flox}$ SFTPC-Cre-^{ERT2} $KFP^{T/+}$ and $Trf1^{+/+}$ SFTPC-Cre-^{ERT2} $KFP^{T/+}$ mice were i.p. inoculated with 50 μl (1 mg per injection) TMX solution three times per week for 6 weeks.

that telomere dysfunction impairs lung stem function by inducing senescence, ultimately leading to an inflammatory response and susceptibility to lung injury, although in this model, the authors did not observe the development of pulmonary fibrosis, most likely because they challenged mice with a high dose of bleomycin (>1 mg/kg BW) (Alder et al., 2015). In this scenario, over 60% of the mice, including wild-type controls, died during the first 2 weeks due to acute epithelial injury, indicating that the DNA damage burden was too high and incompatible with life. The authors did not address the effect of $Trf2$ deletion in adulthood without any additional challenge with bleomycin (Alder et al., 2015).

Together, these findings support a model for the pathobiology of human disease by which persistent DNA damage steaming from short or dysfunctional telomeres associated with either telomere syndromes or organismal aging can synergize with additional cellular damage in order to trigger pulmonary fibrosis (Figure 6). We also show that a high burden of telomeric DNA damage induced by severe telomere dysfunction, in the absence of telomere shortening, is sufficient to trigger pulmonary fibrosis in the absence of any additional

Bleomycin Titration and Inoculation

Decreasing bleomycin concentrations (2.5 mg/kg BW, 1 mg/kg BW, 0.5 mg/kg BW, and 0.1 mg/kg BW) were intratracheally inoculated into 8- to 10-week-old wild-type mice. 2 weeks after the inoculation, mice were sacrificed and analyzed by immunohistochemistry for pulmonary fibrosis.

A low dose of bleomycin (0.5 mg/kg BW) or PBS was inoculated into 8- to 10-week-old wild-type, G2 $Tert^{-/-}$, and G4 $Tert^{-/-}$ mice.

Histopathology, Immunohistochemistry, and Immunofluorescence Analysis

Histopathological analysis of paraffin-embedded lungs was performed in lung sections stained with H&E and Masson trichrome using standard procedures. To quantify collagen deposition, sirius red staining was performed on deparaffinized slides with picrosirius red solution for 1 hr (Broytman et al., 2015).

Immunohistochemistry stainings were performed with the following primary antibodies: rat monoclonal to p53 (POE316A/E9; CNIO histopathology core unit), rat monoclonal to p21 (HUGO-291H/B5; CNIO histopathology core unit), mouse monoclonal to phospho-histone H2AX (Ser139) (Millipore), rat monoclonal to F4/80 (ABD Serotec), p19ARF (5-C3-1 Santa Cruz Biotechnology), activated caspase-3 (R&D Systems), interleukin-6 (ab6672, Abcam), and rabbit polyclonal turbo-RFP (Evrogen).

For immunofluorescence, the antibodies used were a rabbit polyclonal anti-TRF1 (homemade), phospho-H2AX Ser 139 (05-636, Millipore), goat polyclonal anti SPC (C-19, Santa Cruz Biotechnology), α-SMA (CME 305, Biocare Medical), and mouse monoclonal anti *KFP* (RF5R, Abcam). Images were obtained using a confocal ultraspectral microscope (Leica TCS-SP5). Fluorescence intensities were analyzed with Definiens software.

Lung In Vivo Imaging by CT

The acquisition was made on a high-resolution CT system (CT Locus, GE Healthcare) specially designed for small laboratory animals. Mice were anesthetized with a 4% rate of isoflurane (IsoVet Braun) during the induction and 2% during the maintenance period (scanning time). Micro-CT image acquisition consisted of 400 projections collected in one full rotation of the gantry during ~14 min in a single bed focused on the legs, with a 450-μA/80-kV X-ray tube. 2D and 3D images were obtained and analyzed using the software program MicroView (GE Healthcare). All procedures were carried out according to the European Normative of Welfare and Good Practice (2010/63/UE).

Spirometry Analysis

Wild-type and G2 $Tert^{-/-}$ mice were placed into a head-out single chamber plethysmograph (Harvard Apparatus) for 3–5 min. Data acquisition was performed by Pulmodyn W software (from Hugo Sachs Elektronic Harvard Apparatus).

Transcriptional Analysis in Paraffin-Embedded Lungs

RNA was extracted from two lung paraffin block sections of 20 mm with a RNeasy FFPE kit following the manufacturer's instructions (QIAGEN, catalog number 73504). cDNA was synthesized, and collagen I and III expression was analyzed by qPCR. The primers used for Col1a1 were Col1a-F (5′-GCCACTCT GACTGGAAGAGC-3′) and Col1a-R (5′-CAGCCTTGGTTAGGGTCGAT-3′). The primers used for Col3a1 were Col3a1-F (5′AAATTCTGCCACCCCGAACT-3′) and Col3a-R (5′-AGCCTTGGTTAGGATCAACCC-3′).

Telomere Analysis

qFISH determination on paraffin-embedded tissue sections was performed as described previously (González-Suárez et al., 2000). After deparaffinization, tissues were post-fixed in 4% formaldehyde for 5 min, washed three times (5 min each) in PBS, and incubated at 37°C 15 min in pepsin solution (0.1% porcine pepsin, Sigma; 0.01 M HCl, Merck). After another round of washes and fixation as previously mentioned, slides were dehydrated in a 70%-90%-100% ethanol series (5 min each). After 10 min of air-drying, 30 μl telomere probe mix (10 mM TrisCl [pH 7], 25 mM MgCl$_2$, 9 mM citric acid, 82 mM Na$_2$HPO$_4$, 70% deionized formamide [Sigma], 0.25% blocking reagent [Roche], and 0.5 μg/ml telomeric PNA probe [Panagene]) was added to each slide. A coverslip was added, and slides were incubated for 3 min at 85°C and for an additional 2 hr at room temperature in a wet chamber in the dark.

Slides were washed two times (15 min each) in 10 mM TrisCl (pH 7), and 0.1% BSA in 70% formamide under vigorous shaking and three times (5 min each) in TBS 0.08% Tween20 and then incubated in a DAPI bath (4 μg/ml DAPI [Sigma] in PBS) before mounting samples in Vectashield (Vector). Confocal images were acquired as stacks every 1 μm for a total of 3 μm using a Leica SP5-MP confocal microscope, and maximum projections were done with the LAS-AF software. Telomere signal intensity was quantified using Definiens software.

Statistical Analysis

An unpaired Student's t test was used to calculate statistical significance of p21, p53, p19, C3a, and γH2AX markers by immunohistochemistry and interstitial fibrosis by sirius red staining. A log-rank test was used to calculate the statistical differences in the survival curves of the different mice cohorts.

REFERENCES

Alder, J.K., Chen, J.J., Lancaster, L., Danoff, S., Su, S.C., Cogan, J.D., Vulto, I., Xie, M., Qi, X., Tuder, R.M., et al. (2008). Short telomeres are a risk factor for idiopathic pulmonary fibrosis. Proc. Natl. Acad. Sci. USA *105*, 13051–13056.

Alder, J.K., Guo, N., Kembou, F., Parry, E.M., Anderson, C.J., Gorgy, A.I., Walsh, M.F., Sussan, T., Biswal, S., Mitzner, W., et al. (2011). Telomere length is a determinant of emphysema susceptibility. Am. J. Respir. Crit. Care Med. *184*, 904–912.

Alder, J.K., Barkauskas, C.E., Limjunyawong, N., Stanley, S.E., Kembou, F., Tuder, R.M., Hogan, B.L., Mitzner, W., and Armanios, M. (2015). Telomere dysfunction causes alveolar stem cell failure. Proc. Natl. Acad. Sci. USA *112*, 5099–5104.

Armanios, M. (2013). Telomeres and age-related disease: how telomere biology informs clinical paradigms. J. Clin. Invest. *123*, 996–1002.

Armanios, M., and Blackburn, E.H. (2012). The telomere syndromes. Nat. Rev. Genet. *13*, 693–704.

Armanios, M.Y., Chen, J.J., Cogan, J.D., Alder, J.K., Ingersoll, R.G., Markin, C., Lawson, W.E., Xie, M., Vulto, I., Phillips, J.A., 3rd., et al. (2007). Telomerase mutations in families with idiopathic pulmonary fibrosis. N. Engl. J. Med. *356*, 1317–1326.

Beier, F., Foronda, M., Martinez, P., and Blasco, M.A. (2012). Conditional TRF1 knockout in the hematopoietic compartment leads to bone marrow failure and

recapitulates clinical features of dyskeratosis congenita. Blood *120*, 2990–3000.

Blackburn, E.H. (2001). Switching and signaling at the telomere. Cell *106*, 661–673.

Blasco, M.A. (2005). Telomeres and human disease: ageing, cancer and beyond. Nat. Rev. Genet. *6*, 611–622.

Blasco, M.A. (2007). Telomere length, stem cells and aging. Nat. Chem. Biol. *3*, 640–649.

Blasco, M.A., Lee, H.W., Hande, M.P., Samper, E., Lansdorp, P.M., DePinho, R.A., and Greider, C.W. (1997). Telomere shortening and tumor formation by mouse cells lacking telomerase RNA. Cell *91*, 25–34.

Broytman, O., Braun, R.K., Morgan, B.J., Pegelow, D.F., Hsu, P.N., Mei, L.S., Koya, A.K., Eldridge, M., and Teodorescu, M. (2015). Effects of chronic intermittent hypoxia on allergen-induced airway inflammation in rats. Am. J. Respir. Cell Mol. Biol. *52*, 162–170.

Canela, A., Vera, E., Klatt, P., and Blasco, M.A. (2007). High-throughput telomere length quantification by FISH and its application to human population studies. Proc. Natl. Acad. Sci. USA *104*, 5300–5305.

Chong, L., van Steensel, B., Broccoli, D., Erdjument-Bromage, H., Hanish, J., Tempst, P., and de Lange, T. (1995). A human telomeric protein. Science *270*, 1663–1667.

Collado, M., Blasco, M.A., and Serrano, M. (2007). Cellular senescence in cancer and aging. Cell *130*, 223–233.

de Lange, T. (2005). Shelterin: the protein complex that shapes and safeguards human telomeres. Genes Dev. *19*, 2100–2110.

Degryse, A.L., Xu, X.C., Newman, J.L., Mitchell, D.B., Tanjore, H., Polosukhin, V.V., Jones, B.R., McMahon, F.B., Gleaves, L.A., Phillips, J.A., 3rd., et al. (2012). Telomerase deficiency does not alter bleomycin-induced fibrosis in mice. Exp. Lung Res. *38*, 124–134.

Desai, T.J., Brownfield, D.G., and Krasnow, M.A. (2014). Alveolar progenitor and stem cells in lung development, renewal and cancer. Nature *507*, 190–194.

Diéguez-Hurtado, R., Martín, J., Martínez-Corral, I., Martínez, M.D., Megías, D., Olmeda, D., and Ortega, S. (2011). A Cre-reporter transgenic mouse expressing the far-red fluorescent protein Katushka. Genesis *49*, 36–45.

Dobbs, L.G. (1990). Isolation and culture of alveolar type II cells. Am. J. Physiol. *258*, L134–L147.

Ferrón, S., Mira, H., Franco, S., Cano-Jaimez, M., Bellmunt, E., Ramírez, C., Fariñas, I., and Blasco, M.A. (2004). Telomere shortening and chromosomal instability abrogates proliferation of adult but not embryonic neural stem cells. Development *131*, 4059–4070.

Flores, I., Cayuela, M.L., and Blasco, M.A. (2005). Effects of telomerase and telomere length on epidermal stem cell behavior. Science *309*, 1253–1256.

Flores, I., Canela, A., Vera, E., Tejera, A., Cotsarelis, G., and Blasco, M.A. (2008). The longest telomeres: a general signature of adult stem cell compartments. Genes Dev. *22*, 654–667.

García-Cao, I., García-Cao, M., Martín-Caballero, J., Criado, L.M., Klatt, P., Flores, J.M., Weill, J.C., Blasco, M.A., and Serrano, M. (2002). "Super p53" mice exhibit enhanced DNA damage response, are tumor resistant and age normally. EMBO J. *21*, 6225–6235.

González-Suárez, E., Samper, E., Flores, J.M., and Blasco, M.A. (2000). Telomerase-deficient mice with short telomeres are resistant to skin tumorigenesis. Nat. Genet. *26*, 114–117.

Greider, C.W., and Blackburn, E.H. (1985). Identification of a specific telomere terminal transferase activity in Tetrahymena extracts. Cell *43*, 405–413.

Harley, C.B., Futcher, A.B., and Greider, C.W. (1990). Telomeres shorten during ageing of human fibroblasts. Nature *345*, 458–460.

Herrera, E., Samper, E., Martín-Caballero, J., Flores, J.M., Lee, H.W., and Blasco, M.A. (1999). Disease states associated with telomerase deficiency appear earlier in mice with short telomeres. EMBO J. *18*, 2950–2960.

Hinz, B., Phan, S.H., Thannickal, V.J., Galli, A., Bochaton-Piallat, M.L., and Gabbiani, G. (2007). The myofibroblast: one function, multiple origins. Am. J. Pathol. *170*, 1807–1816.

King, T.E., Jr., Pardo, A., and Selman, M. (2011). Idiopathic pulmonary fibrosis. Lancet *378*, 1949–1961.

Lama, V.N. (2009). Update in lung transplantation 2008. Am. J. Respir. Crit. Care Med. *179*, 759–764.

Lee, H.W., Blasco, M.A., Gottlieb, G.J., Horner, J.W., 2nd, Greider, C.W., and DePinho, R.A. (1998). Essential role of mouse telomerase in highly proliferative organs. Nature *392*, 569–574.

Leri, A., Franco, S., Zacheo, A., Barlucchi, L., Chimenti, S., Limana, F., Nadal-Ginard, B., Kajstura, J., Anversa, P., and Blasco, M.A. (2003). Ablation of telomerase and telomere loss leads to cardiac dilatation and heart failure associated with p53 upregulation. EMBO J. *22*, 131–139.

Liu, Y., Snow, B.E., Hande, M.P., Yeung, D., Erdmann, N.J., Wakeham, A., Itie, A., Siderovski, D.P., Lansdorp, P.M., Robinson, M.O., and Harrington, L. (2000). The telomerase reverse transcriptase is limiting and necessary for telomerase function in vivo. Curr. Biol. *10*, 1459–1462.

Liu, T., Chung, M.J., Ullenbruch, M., Yu, H., Jin, H., Hu, B., Choi, Y.Y., Ishikawa, F., and Phan, S.H. (2007). Telomerase activity is required for bleomycin-induced pulmonary fibrosis in mice. J. Clin. Invest. *117*, 3800–3809.

López-Otín, C., Blasco, M.A., Partridge, L., Serrano, M., and Kroemer, G. (2013). The hallmarks of aging. Cell *153*, 1194–1217.

Martínez, P., Thanasoula, M., Muñoz, P., Liao, C., Tejera, A., McNees, C., Flores, J.M., Fernández-Capetillo, O., Tarsounas, M., and Blasco, M.A. (2009). Increased telomere fragility and fusions resulting from TRF1 deficiency lead to degenerative pathologies and increased cancer in mice. Genes Dev. *23*, 2060–2075.

Martinez, F.J., de Andrade, J.A., Anstrom, K.J., King, T.E., Jr., and Raghu, G.; Idiopathic Pulmonary Fibrosis Clinical Research Network (2014). Randomized trial of acetylcysteine in idiopathic pulmonary fibrosis. N. Engl. J. Med. *370*, 2093–2101.

Mouratis, M.A., and Aidinis, V. (2011). Modeling pulmonary fibrosis with bleomycin. Curr. Opin. Pulm. Med. *17*, 355–361.

Rawlins, E.L. (2015). Stem cells: Emergency back-up for lung repair. Nature *517*, 556–557.

Rock, J.R., Barkauskas, C.E., Cronce, M.J., Xue, Y., Harris, J.R., Liang, J., Noble, P.W., and Hogan, B.L. (2011). Multiple stromal populations contribute to pulmonary fibrosis without evidence for epithelial to mesenchymal transition. Proc. Natl. Acad. Sci. USA *108*, E1475–E1483.

Ryu, J.H., Moua, T., Daniels, C.E., Hartman, T.E., Yi, E.S., Utz, J.P., and Limper, A.H. (2014). Idiopathic pulmonary fibrosis: evolving concepts. Mayo Clin. Proc. *89*, 1130–1142.

Schneider, R.P., Garrobo, I., Foronda, M., Palacios, J.A., Marión, R.M., Flores, I., Ortega, S., and Blasco, M.A. (2013). TRF1 is a stem cell marker and is essential for the generation of induced pluripotent stem cells. Nat. Commun. *4*, 1946.

Selman, M., King, T.E., and Pardo, A.; American Thoracic Society; European Respiratory Society; American College of Chest Physicians (2001). Idiopathic pulmonary fibrosis: prevailing and evolving hypotheses about its pathogenesis and implications for therapy. Ann. Intern. Med. *134*, 136–151.

Stanley, S.E., Chen, J.J., Podlevsky, J.D., Alder, J.K., Hansel, N.N., Mathias, R.A., Qi, X., Rafaels, N.M., Wise, R.A., Silverman, E.K., et al. (2015). Telomerase mutations in smokers with severe emphysema. J. Clin. Invest. *125*, 563–570.

Van der Velden, J.L., Bertoncello, I., and McQualter, J.L. (2013). LysoTracker is a marker of differentiated alveolar type II cells. Respir. Res. *14*, 123.

Vera, E., Bernardes de Jesus, B., Foronda, M., Flores, J.M., and Blasco, M.A. (2012). The rate of increase of short telomeres predicts longevity in mammals. Cell Rep. *2*, 732–737.

Zhang, H.Y., Gharaee-Kermani, M., Zhang, K., Karmiol, S., and Phan, S.H. (1996). Lung fibroblast alpha-smooth muscle actin expression and contractile phenotype in bleomycin-induced pulmonary fibrosis. Am. J. Pathol. *148*, 527–537.